

THE SECOND *GALEX* ULTRAVIOLET VARIABILITY (GUVV-2) CATALOG

Jonathan M. Wheatley,¹ Barry Y. Welsh,¹ and Stanley E. Browne¹

ABSTRACT

We present the second Galaxy Evolution Explorer (*GALEX*) Ultraviolet Variability (GUVV-2) Catalog that contains information on 410 newly discovered time-variable sources gained through simultaneous near (NUV 1750 - 2750 Å) and far (FUV 1350 - 1750 Å) ultraviolet photometric observations. Source variability was determined by comparing the NUV and/or FUV fluxes derived from orbital exposures recorded during a series of multiple observational visits to 169 *GALEX* fields on the sky. These sources, which were contained within a sky-area of 161 deg², varied on average by $\Delta\text{NUV} = 0.6$ mag and $\Delta\text{FUV} = 0.9$ mag during these observations. Of the 114 variable sources in the catalog with previously known identifications, $\sim 67\%$ can be categorized as being active galaxies (QSO's, Seyfert 1 or BL Lac objects). The next largest groups of UV variables are RR Lyrae stars, X-ray sources and novae.

By using a combination of UV and visible color-color plots we have been able to tentatively identify 36 possible RR Lyrae and/or δ Scuti type stars, as well as 35 probable AGN's, many of which may be previously unidentified QSO's or blazars. Finally, we show data for 3 particular variable objects: the contact binary system of SDSS J141818.97+525006.7, the eclipsing dwarf nova system of IY UMa and the highly variable unidentified source SDSS J104325.06+563258.1.

Subject headings: stars : variables — other: galaxies — ultraviolet: general

1. Introduction

The NASA Galaxy Evolution Explorer (*GALEX*) satellite, launched on 2003 April 28th, is currently making imaging photometric observations of the sky in two ultraviolet bands (NUV 1750 - 2750Å , FUV 1350 - 1750Å). A summary of the main scientific findings obtained during the first year of its on-orbit operation can be found in (Martin et al. 2005) and

¹Experimental Astrophysics Group, Space Sciences Laboratory, University of California, 7 Gauss Way, Berkeley, CA 94720; wheat@ssl.berkeley.edu, bwelsh@ssl.berkeley.edu, seb@ssl.berkeley.edu

references therein. Repeated (i.e. multi-orbit) observations of selected areas of the sky are made in the Deep Imaging Survey (DIS) (Morrissey et al. 2005, 2007) and in certain Guest Investigator (GI) observations. This observing strategy requires making repeated visits to the same position on the sky with the 1.2° instrument field of view, thus enabling numerous astronomical sources to have their FUV and NUV fluxes to be determined at many different epochs. From these observations it is thus possible to detect variable ultraviolet sources, many of which exhibit much larger amplitudes of variation in the ultraviolet region than that typically found at visible wavelengths. A list of 84 time-variable UV sources discovered during the first 14 months of the *GALEX* mission (i.e. 2003 June to 2004 August) has been presented by Welsh et al. (2005) in version 1.0 of the *GALEX* Ultraviolet Variability (GUVV) Catalog. The great majority of these 84 UV variable objects were found to be either RR Lyrae or dMe flare stars, together with a few Delta Scuti and X-ray variable objects. Since the publication of the first GUVV catalog several papers have been published on the more extreme cases of UV source variability, such as the *GALEX* high time-resolution (< 1 sec) observations of flares on 4 nearby dMe stars (Welsh et al. 2006) and the large amplitude UV variations found for the RR Lyrae star ROTSE-I J143753.84+345924.8 (Wheatley et al. 2005). We note that the observation of flux variability in astronomical objects can provide important constraints on the physical processes responsible for the observed emission, especially in the cases of X-ray/UV emission from highly energetic sources such as AGN and black hole candidates.

In this Paper we report on the analysis of new *GALEX* observations of 169 sky-fields performed during the 2003 June to 2006 June timeframe. Each sky-field was observed at least 10 times, each for a period of 1200 sec to 1700 sec. We report on 410 newly discovered UV variable sources which will subsequently require follow-up observations in other wavelength bands in order to fully describe the true physical nature associated with the variability of each of the listed sources.

2. Observations and Data Analysis

We have used the *GALEX* FUV and NUV-band photometric data catalogs compiled during the period 2003 June to 2006 June, which reside in the Multi-Mission Archive at the Space Telescope Science Institute (MAST). Only the *GALEX* fields observed on 10 or more occasions (and with exposures of more than 200 sec) were included in our present analysis. A list of each sky-field, together with the number of separate observations (or ‘exposures’), is given in Table 1 and the distribution of these fields on the sky is shown in Figure 1. Since the prime scientific reason for selecting these fields was to carry out *GALEX* UV observations of

galaxies and/or galaxy clusters, it is not surprising that the vast majority of these sky-fields are located away from the galactic plane such that saturation of the detectors due to overly-bright stellar sources and the effects of interstellar absorption in the galactic plane are both minimized.

The data files for each exposure of the 169 1.2° diameter sky-fields contain photon events that have been processed using the standard *GALEX* Data Analysis Pipeline operated at the Caltech Science Operations Center (Pasadena, CA). This pipeline ingests time-tagged photon lists, instrument and spacecraft housekeeping data and satellite pointing aspect information (Morrissey et al. 2007). The data pipeline then uses a source detection algorithm called SExtractor (Bertin & Arnouts 1996) to produce a catalog of source positions on the sky with corresponding FUV and NUV source magnitudes calculated for each observational visit. Source magnitudes derived from use of a fixed 12 arcsec diameter aperture with SExtractor were utilized in this study, since these are more appropriate for isolating flux from stellar sources rather than galaxies. The source detections within each exposure at each sky-field position on the sky appear as source lists in the *GALEX* archival database of the MAST.

Comparison software was then run on the MAST source list catalog to reveal objects that we deemed as being time-variable. This procedure involved the following 4 steps that were applied to each of the individual exposures of every source detected within each of the 169 sky-fields: (1) Firstly, only objects brighter than NUV magnitude $m_{NUV} = 21.0$, that were also located within 0.55 degrees of the center of each *GALEX* field were selected. Such a choice lessens the influence of both degraded image resolution and ‘detector edge effects’ that can potentially cause artifacts in the data. The choice of magnitude limit was based on ultimately being able to maximize the number of truly variable sources while minimizing a far larger number of spuriously variable fainter sources. Targets within this selected area that were flagged by the *GALEX* pipeline as being potential image artifacts in the MAST data-set were also rejected. The result from this search was a list of sources, sky positions and values of NUV (and FUV) magnitude that were found within each exposure associated with each of the 169 sky-fields. (2) A comparison was then performed on all values of m_{NUV} that were obtained for each source from the various exposures of each of the sky-fields. Since the listed source positions each have an inherent measurement error of $\sim \pm 3$ arc sec (Morrissey et al. 2005), we restricted the comparison to sources listed within a 10 arc sec diameter error circle of the nominal source position. Only sources that varied by > 0.6 NUV magnitudes within this error circle were selected as being potentially time-variable. This variability criterion corresponds to a $> 3\sigma$ change in the photon statistical error assigned to each source by the *GALEX* data pipeline. However, we note that for faint sources the *GALEX* systematic error (which is due to the combined effects of sky-subtraction, flat fielding and scattered light subtraction) is far larger than the photon statistical error

(Morrissey et al. 2005). Thus, the choice of > 0.6 NUV mag. significantly minimizes the number of false variability detections. We note that the photometric stability of *GALEX* assessed during the 2003 - 2006 period is < 0.1 magnitudes (Morrissey et al. 2007). (3) When available, a comparison was also made with the corresponding FUV magnitudes, m_{FUV} , for each exposure of the sources previously identified in Step (2). If the selected source *also* varied by > 0.4 FUV magnitudes, then this was deemed a confirmation of true source variability. In cases where no FUV data were available, Step (3) was omitted. (4) The previous two steps resulted in a list of NUV (and/or FUV) source magnitudes with their associated sky positions recorded at a given epoch for each exposure of the various sky-fields. Each of these source lists was then plotted (as epoch versus magnitude) and the individual light-curves visually checked for the plausibility of astronomical source variability. The images of individual GALEX visits were also visually checked as a final verification that the source flux variation was not caused by some image anomaly. A typical anomaly in GALEX images is scattered light leakage caused by bright objects positioned just outside of the instrument field-of-view. In Figure 2 we show two GALEX images recorded for the ELAIS-N1 field, taken 2.5 months apart. The fuzzy horseshoe-like feature to the left of center of the 2005 May 3rd image is due to scattered light and is seen to re-appear in the 2005 July 24th image with a greatly reduced intensity at a different angle to the two central bright objects, due to the different roll angle used in this pointing of the GALEX instrument. Finally, we also ran a search for FUV source variability that was not accompanied by any appreciable NUV variability. This entailed running Steps (1) and (2) within the constraints of $m_{FUV} < 22.0$ and an FUV magnitude variation of > 1.0 magnitude.

The list of 410 resultant time-variable UV sources is given in Table 2. In column (1), following the format of the GUVV-1 catalog (Welsh et al. 2005), we list a unique identifier for each source that contains its *GALEX* mean right ascension (J2000.0) in hours, minutes and decimal seconds and its corresponding declination (J2000.0) in degrees, arcminutes and decimal seconds. In column (2) we list, when available, the USNO-B1.0 all-sky catalog designation in *italics* (Monet et al. 2003) or the Sloan Digital Sky Survey DR6 designation in Roman typeface (Adelman-McCarthy et al. 2007). For objects that appear in the SIMBAD on-line astronomical catalog, in column (3) we list their source identification. In column (4) we list, when known, the most likely astronomical source-type for the source. Criteria used to make this latter determination were generally varied, but (for the brighter sources) are mainly based on either their Simbad catalog identifications or on inspection of their *GALEX* UV light-curve data (gained from Step 4 of the data search). The majority of these variable sources have no known associated source type, but when known we list source types in the following 11 categories: QSO's (quasar stellar objects), Sy1 (Seyfert 1 galaxies), AGN (active galactic nuclei), BLL (BL Lacs), Gal (ordinary galaxies), RR* (RR Lyrae stars), X (X-ray

sources), V* (variable star), ** (double stars), Nov (novae and dwarf novae) and Fl* (dMe flare stars).

In column (5) we list the name of the *GALEX* sky-field in which the variable source was found. In column (6) we list the total number of detections (NUV_{det}) of the variable source within the associated set of NUV observations of the *GALEX* sky-field. Column (8) lists the maximum observed NUV magnitude (NUV_{max}) for the source (measured in a single exposure) and column (9) lists the variation between the corresponding maximum and minimum NUV magnitudes (i.e. ΔNUV). Similarly, columns (10) - (13) list the equivalent number of detections (FUV_{det}), maximum magnitude (FUV_{max}) and variation in magnitude (ΔFUV) for the FUV channel. We emphasize that the non-detection of a source previously observed in both (or one) of the two UV-bands can be attributed to either intrinsic variability (i.e. an astrophysical effect) or being due to one of the detectors having been turned off during a particular observation for instrument safety reasons. Finally, in columns (14) - (16) we list (in Roman typeface) the respective g , r and i photometric PSF magnitudes as recorded by the Sloan Digital Sky Survey (SDSS) catalog (Adelman-McCarthy et al. 2007) for the source designation listed in column (2). Finally, we note that this new GUVV-2 catalog also includes some of the variable sources listed in the GUVV-1 catalog, often with different magnitude changes. This is due to either a greater number of observations per source being presently available for analysis, or the improvement in the source detection algorithms of Version 5.1 of the *GALEX* data pipeline software. For sources that have no or uncertain SDSS photometric magnitudes, we list the available USNO-B B, R and I magnitudes in *italics*.

3. Discussion

In this section we analyze some of the statistical properties of the 410 UV variable sources listed in Table 2. The present sample of variable sources has been discovered through observations covering a total area of $\sim 161 \text{ deg}^2$ on the sky, with the vast majority of the fields being located at galactic latitudes well away from the galactic plane. The previous GUVV-1 study of Welsh et al. (2005) detected 84 variable sources contained within a far larger area on the sky of $\sim 3000 \text{ deg}^2$. The larger area covered was due to the use of many All-Sky Imaging Survey (AIS) fields recorded during the initial survey phase of the *GALEX* mission. The current GUVV-2 detection rate is ~ 2.6 variable UV sources per deg^2 . This can be directly compared with a GUVV-1 detection rate from DIS pointings of ~ 1.2 variable sources per deg^2 gained from observations of 15 deg^2 . The increase in the present detection rate is due to improved variability search software and the generally longer time series of

exposures over which variability could be assessed within the presently observed fields.

3.1. Variability Statistics

In Figure 3 we plot the respective maximum changes in UV magnitude, NUV_{max} and FUV_{max} , as a function of the number of sources exhibiting such variability. Although we see a maximum number of NUV variable sources with $\Delta NUV = 0.6$ mag, the sharp cut-on in this source distribution is due to our definition of NUV variability as being greater than 0.6 mag. Unfortunately selecting an NUV magnitude variability less than this value results in a very large number of false detections, particularly for sources with NUV magnitudes fainter than $NUV = 19.0$. In the case of (associated) FUV source variability we see a maximum number of sources at $\Delta FUV = 0.9$ mag. In Figure 4 we plot values of NUV_{max} versus FUV_{max} for these sources and find that the great majority of targets lie within ± 1 mag of a straight line of slope +0.91. This is very similar to the results found for the far smaller sample of UV variable sources in the GUVV-1 catalog (Welsh et al. 2005). We note the large number of sources with peak FUV and NUV magnitudes > 20.0 that deviate more than this value from the best-fit line, and this is due to the larger measurement errors associated with these faint sources.

Of the 410 variable sources in Table 2 only 114 have astronomical identifications listed in the Simbad database. Of these sources, 77 (i.e. 67%) can be categorized as active galaxies (i.e. QSO's, AGN, BLL or Sy1). The next largest groups are those of X-ray sources (19), RR Lyrae stars (6) and Novae (3). Although active galaxies are the largest group of *identified* sources, it is highly probable that many of the remaining 296 uncategorized variable sources are of a stellar origin. This is mainly due to the poor coverage of astronomical identifications in the SIMBAD database for faint stellar sources as opposed to that for active galaxies.

3.2. RR Lyrae Stars

GALEX has been shown to be a sensitive probe of the flux variability observed towards RR Lyrae stars, since these stars can vary by up to 6 magnitudes at FUV wavelengths (Wheatley et al. 2005). Using the known UV variable sources listed in the GUVV-1 catalog, Browne (2005) found that plots of $(g - r)$ versus $(u - g)$ SDSS magnitudes revealed a segregation of stellar sources that could be readily identified with RR Lyrae and δ Scuti-type stars. In Figure 5 we have produced a similar plot of $(g - r)$ versus $(u - g)$ SDSS magnitudes for the present GUVV-2 set of variable sources listed in Table 2. The box drawn on this

Figure (i.e. $0.99 < (u - g) < 1.28$ and $-0.20 < (g - r) < +0.31$) contains 36 sources, all of which are listed separately in Table 3. Only 2 of these sources are previously known RR Lyrae stars (i.e. HL Her and V851 Her), and in Figure 7(a) we show the magnitude-phase light curve for the newly discovered RR Lyrae star, SDSS J081226.4+033320.1 that has a period of 0.555 days. This type of UV observation, when used in conjunction with ground-based ROTSE data, can be used to constrain Kurucz stellar atmosphere model parameters such as stellar temperature and metallicity for RR Lyrae stars (Wheatley et al. 2005). Finally, we note that Table 2 also lists 4 previously known RR Lyrae stars (with SIMBAD identifications) that are not shown in Figure 5. These stars, which have had their RR Lyrae status confirmed by other means, have not been included in Table 3 since their SDSS color magnitudes are not available..

3.3. AGN and QSO's

As previously stated, the largest group of known UV variable sources in Table 2 are active galaxies. Quasars, blazars, BL Lac and Seyfert galaxies have long been known to exhibit flux variability at all observed wavelengths from radio to gamma-rays, lasting over time-scales of weeks, days or hours (micro-variability). Flux variability studies, particularly at X-ray wavelengths, have been used to provide clues to the sizes and structure of the emission regions producing the observed variable level of radiation. The non-thermal emission from the nuclei of active galaxies reveals itself as a flat UV-to-optical continuum spectrum, with the probable origin of the nuclear activity arising around a supermassive black hole situated in the centre of the host galaxy which accretes gas from the host. During this process, gravitational binding energy is released, part of which is transformed into the UV radiation observed by GALEX. A typical UV spectrum of a low red-shift blazar is given in Pian, Falomo & Treves (2005), with the majority of the flux being contained in the emission lines of SiIV, CIV and CIII superposed on an underlying continuum in the GALEX FUV channel. The GALEX NUV channel contains no strong emission lines with only UV continuum emission being observed from these sources.

Although we are presently unable to positively determine which of the sources listed in Table 2 are true blazars, since the number of presently known objects is small (especially so for the southern galactic hemisphere), we believe it useful to produce a list of possible blazar candidates for subsequent study and confirmation at other wavelengths. Both Seibert et al. (2005) and Bianchi et al. (2007) have attempted to isolate low red-shift QSO candidate sources in the GALEX data archive from color-color diagrams that use both UV and SDSS color magnitudes. In particular, plots of $(m_{FUV} - m_{NUV})$ versus $(m_{NUV} - r)$ colors can

provide a very helpful discriminant between hot UV bright stars and low red-shift QSO's. In Figure 6 we show such a color-color plot for all objects in Table 2 that possess both an SDSS r color magnitude and which exhibit variability in both the FUV and NUV channels. Sources previously identified as QSO's in SIMBAD are plotted as filled circles, and those without previous identification are plotted as open circles. Following the work of Seibert et al. (2005) and Bianchi et al. (2007), it is highly probable that sources lying within the region bounded by $-0.5 < (FUV_{max} - NUV_{max}) < +1.5$ and $(NUV_{max} - r) < 2.0$ are low red-shift QSO's or possibly blazars. We have identified these 35 objects in Table 2 (see footnote to Table 2). This sample could possibly be contaminated by a few cataclysmic variable stars but, as discussed in Bianchi et al. (2007), such objects are quite rare compared to the observed space density of QSO's. Finally, we note the the group of sources in Figure 6 that possess $(FUV_{max} - NUV_{max}) > +2$ are most likely to be variable main-sequence objects.

3.4. Some Interesting GUVV-2 objects

Of the 410 objects listed in Table 2, three sources stand out as being of particular interest. These are (i) the contact binary system of SDSS J141818.97+525006.7, (ii) the eclipsing dwarf nova system of IY UMa (SDSS J104356.72+580731.9) and (iii) the highly variable unidentified source SDSS J104325.06+563258.1.

In Figure 7(b) we show the NUV light curve for SDSS J141818.97+525006.7, which is a contact binary system listed in the catalog of Gettel, Geske & McKay (2006). This type of highly evolved system, often referred to as W Ursae Majoris (W UMa) variables, consists of two very close binary stars whose outer atmospheric surfaces share a common envelope. Noting that there are *two* eclipses per cycle in the phased UV light-curve, and we derive a period of 0.29064 d for this system which can be compared with that of 0.29082 d obtained from visible data. Finally, we note that the period for this system is very close to that of 0.27 d, which Rucinski (2007) cites as the maximum of the period distribution for all known W UMa systems.

IY UMa is one of the few known eclipsing dwarf nova systems of the SU UMa-type, consisting of a white dwarf which accretes matter via a Roche lobe flow from a late-type donor star (Uemura et al. 2000). Such systems typically undergo series of both short (days) and long (weeks) outbursts. The GALEX data, shown in Figure 8(a) represent the first UV observations of this system, in which variability of ~ 1 mag. has been detected over a set of several observations spanning ~ 1 year. Previous visible spectrophotometric and spectroscopic observations of this system have revealed both normal and super-outbursts which have been successfully modeled by Patterson et al. (2000) and Rolfe et al. (2005).

Finally, in Figure 8(b) we show sets of NUV and FUV observations of the highly variable source SDSS J104325.06+563258.1 recorded with GALEX over a 24 month time-frame. This source appears to possess FUV and NUV ‘quiescent’ magnitudes of ~ 20 mag, as measured during two observations some 450 days apart, followed by two flare events which caused an increase of > 2 magnitudes. Although the temporal coverage of these outbursts is not contiguous, the data do allow us to note that there was a rise of 3.7 mag in the NUV in 40 days and on one occasion there was a drop of ~ 2.0 mag in both the NUV and FUV channels in only 21 hours. Its SDSS *ugriz* magnitudes are all similar, suggesting a flat spectral shape in the visible region, which would preclude its identification as a flaring M-dwarf star. Although ground-based spectroscopic observations are required to provide a firm identification for this source, it is probably a previously unknown distant dwarf nova system.

3.5. Future Studies

The great majority of the presently detected variable sources will require follow-up spectroscopic study in order to reveal their true physical identity. However, it is clear from the 114 sources that already have previous identifications that the GUVV-2 catalog will be a very useful tool in the study (and identification) of the UV variability of active galaxies.

All of our present variable source detections have been based on their orbit-to-orbit variation in UV magnitude. The present study has not used the photon data from each source to search for variability on time-scales of the order of seconds. Previous studies of time-tagged photon data from 1800 GALEX images have revealed short-term (< 100 sec) UV flare events from 49 newly identified dMe stars (Welsh et al. 2007). Future inspection of the photon data from the entire GALEX data-base could enable studies of a variety of new source phenomenon that includes the possible detection of stellar transits by Jupiter-sized exo-planets and the study of short-term flare outbursts from cataclysmic variable systems.

We gratefully acknowledge NASA’s support for construction, operation, and science analysis for the GALEX mission, developed in cooperation with the Centre National d’Etudes Spatiales of France and the Korean Ministry of Science and Technology. We acknowledge the dedicated team of engineers, technicians, and administrative staff from JPL/Caltech. Financial support for this research was provided by NASA grant NNG06GD17G through the GALEX Guest Investigator program. This publication makes use of data products from the SIMBAD database, operated at CDS, Strasbourg, France, and the Sloan Digital Sky Survey.

REFERENCES

- Adelman-McCarthy, J., Agueros, M., Allam, S. et al., 2007, *ApJS* 172, 634
- Bertin, E. & Arnouts, S., 1996, *A&AS* 117, 393
- Bianchi, L., Rodriguez-Merino, L., Viton, M. et al., 2007, *ApJS* 173, 659
- Browne, S.E., 2005, *PASP*, 117, 726
- Gettel, S., Geske, M. and McKay, T., 2006, *AJ*, 131, 621
- Ivezic, Z., Vivas, A.K., Lupton, R. and Zinn, R., 2005, *AJ*, 129, 1096
- Martin, D.C., et al. 2005, *ApJ*, 619, L1
- Monet, D.G., Levine, S.E., Canzian, B. et al., 2003, *AJ*, 125, 984
- Morrissey, P., Schiminovich, D., Barlow, T. et al., 2005, *ApJ*, 619, 7
- Morrissey, P., Conrow, T., Barlow, T. et al., 2007, *ApJS*, 173, 682
- Patterson, J., Kemp, J., Jensen, L., et al., 2000, *PASP*, 112, 1567
- Paian, E., Falamo, R. and Treves, A., 2005, *MNRAS*, 361, 919
- Rolfe, D., Haswell, C., Abbott, T. et al., 2005, *MNRAS*, 357, 69
- Rucinski, S.M., 2007, *MNRAS*, 382, 39
- Seibert, M., Budavari, T., Rhee, J. et al., 2005, *ApJ*, 619, L23
- Uemura, M., Kato, T., Matsumoto, K. et al., 2000, *PASJ*, 52, L9
- Welsh, B.Y., Wheatley, J.M., Heafield, K. et al., 2005, *AJ*, 130, 825
- Welsh, B.Y., Wheatley, J.M., Browne, S.E. et al., 2006, *A&A*, 458, 921
- Welsh, B.Y., Wheatley, J.M., Seibert, M. et al., 2007, *ApJS*, 173, 673
- Wheatley, J.M., Welsh, B.Y., Siegmund, O.H.W. et al. 2005, *ApJ*, 619, L123

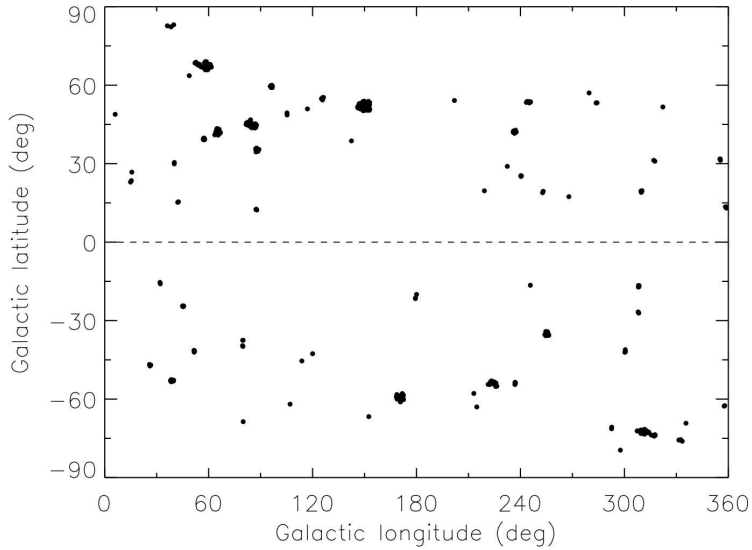


Fig. 1.— Distribution of the GUVV-2 catalogued sources on the sky.

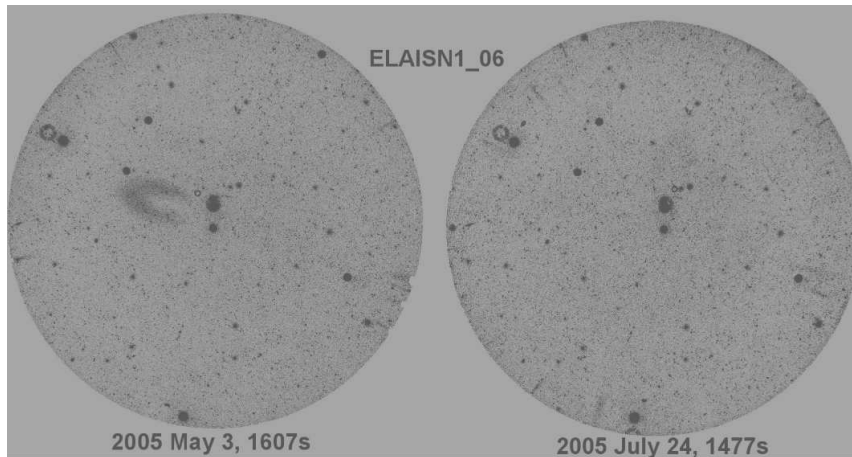


Fig. 2.— Two GALEX NUV images of the sky-field ELAIS-N1 recorded on 2005 May 3rd and 2005 July 24th. Note the fuzzy horseshoe-shaped object to the left of center of the May 3rd image that re-appears in the corresponding July 24th image with a greatly reduced intensity and different orientation angle to the rest of the image. This feature is caused by scattered light-leakage for bright objects lying just beyond the GALEX instrument field-of-view.

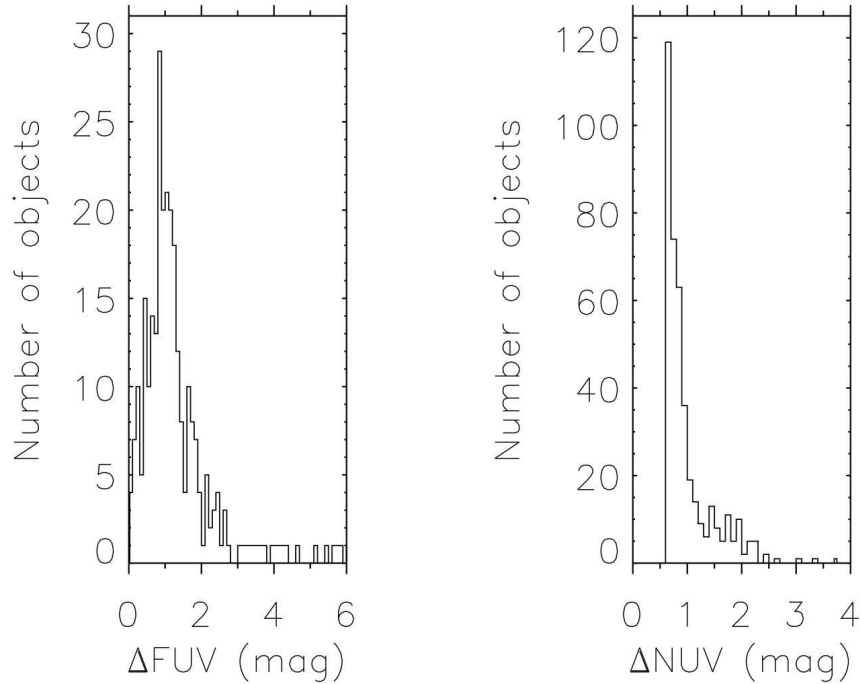


Fig. 3.— Plots of the maximum GALEX magnitudes, FUV_{max} and NUV_{max} , as a function of the number of UV sources exhibiting such variability.

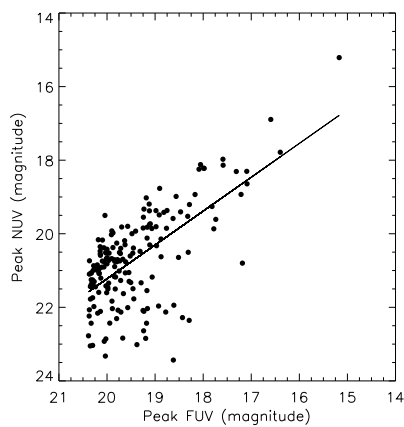


Fig. 4.— Plot of the GALEX FUV peak magnitude vs. the peak NUV magnitude for the GUVV-2 sources listed in Table 2. The majority of sources lie within ± 1 mag of a straight line of slope +0.91.

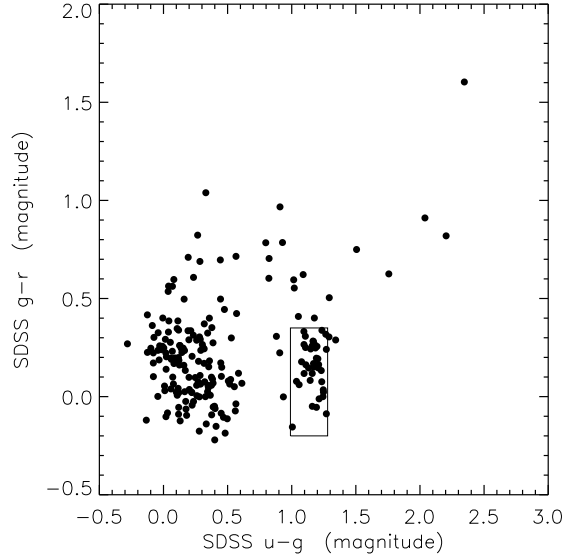


Fig. 5.— Plot of the SDSS ($g - r$) versus ($u - g$) magnitudes for the GUVV-2 catalog sources. The 36 sources contained within the drawn box are most probably either RR Lyrae or δ Scuti-type variables.

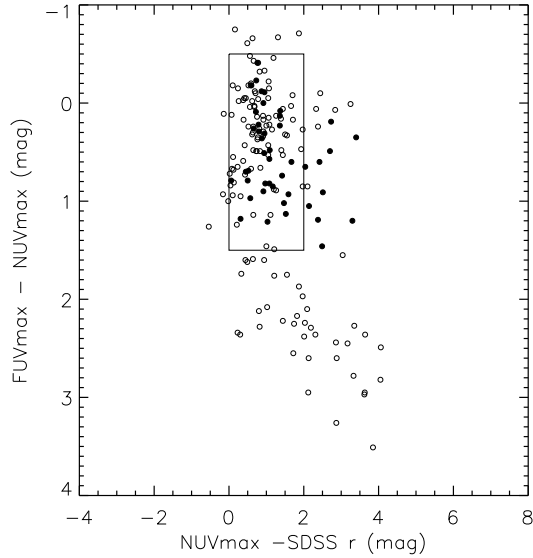


Fig. 6.— Plot of $(FUV_{max} - NUV_{max})$ vs. $(NUV_{max} - SDSS\ r)$ for the variable sources in Table 2. Filled circles are sources previously identified as QSO's, open circles have no current identification. The open circle sources contained with the drawn box are most probably newly identified QSO's, and are marked as PQ (possible QSO's) in column 4 of Table 2.

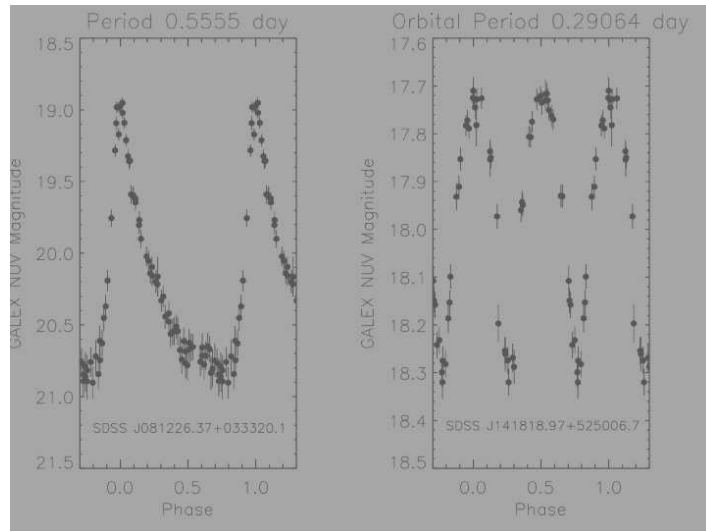


Fig. 7.— (a) Phased UV light-curve for the newly discovered RR Lyrae star, SDSS J081226.4+033320.1 which has an estimated period of 0.555 d . (b) The NUV light curve for the contact binary system SDSS J141818.97+525006.7, which has a derived UV period of 0.29064 d .

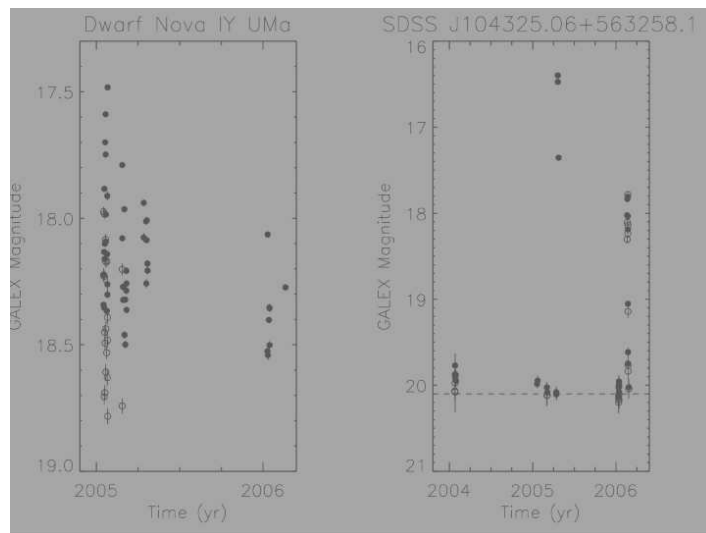


Fig. 8.— (a) Variation in FUV (open circles) and NUV (filled circles) magnitudes for the eclipsing dwarf nova system, IY UMa recorded at several epochs during a period of 12 months. (b) Unusually large variations in both FUV (open circles) and NUV (filled circles) magnitudes for the unidentified source, SDSS J104325.06+563258.1 recorded over a 2 year time-frame.

Table 1. GALEX Fields Analyzed for Variability

Field	Survey	Visits	Right Ascension	Declination
CARINA_DPH	NGS	24	100.36	-51.31
CCS_DSF2237	DIS	20	339.96	11.88
CCS_Q2233	DIS	25	339.04	13.94
CDFS_00	DIS	61	53.13	-27.87
CDFS_01	DIS	21	52.01	-28.21
CDFS_03	DIS	22	54.17	-27.31
CDFS_04	DIS	14	52.93	-28.91
CDFS_05	DIS	14	52.11	-27.28
CDFS_07	DIS	16	52.10	-29.21
CDFS_08	DIS	17	53.10	-29.40
CDFS_09	DIS	14	54.10	-29.03
CDFS_10	DIS	15	52.90	-27.37
CFHTLS4	DIS	50	333.78	-17.94
CNOC2_00	DIS	31	327.51	-5.46
COMBO17_A901	DIS	32	149.09	-10.11
COSMOS_01	DIS	47	150.37	2.46
COSMOS_02	DIS	46	150.37	1.96
COSMOS_03	DIS	58	149.87	2.46
COSMOS_04	DIS	50	149.87	1.96
DEEP23H	DIS	60	352.50	0.00
DEEP23H_01	DIS	54	351.75	0.14
DEEP23H_02	DIS	51	353.27	0.14
DEEP2H	DIS	25	37.15	-0.27
DEEP2H_01	DIS	21	36.89	0.59
DEEPLNS_N1_00	DIS	17	13.67	12.80
DEEPZLE_00	DIS	46	253.01	34.93
DEEPZLE_01	DIS	57	252.00	34.92
DLENSS_00	DIS	20	79.44	-48.99
DLENSS_01	DIS	21	80.70	-48.40
DLENSS_02	DIS	23	79.30	-48.30
DLENSS_03	DIS	22	80.75	-49.05
DLENSS_04	DIS	19	80.70	-49.70
DLENSS_05	DIS	24	79.20	-49.75
EIS_WIDE_D	DIS	14	137.44	-2.52
EISD1AB	DIS	35	343.39	-40.22
ELAISN1_00	DIS	14	243.40	54.98
ELAISN1_01	DIS	13	241.96	55.64
ELAISN1_02	DIS	14	241.72	54.58
ELAISN1_03	DIS	13	245.15	55.89
ELAISN1_04	DIS	13	243.28	53.89
ELAISN1_05	DIS	14	243.16	56.55
ELAISN1_06	DIS	12	241.50	56.61
ELAISN1_07	DIS	12	244.71	55.10
ELAISN1_08	DIS	13	241.01	55.05
ELAISN1_09	DIS	11	241.61	53.53
ELAISN1_10	DIS	11	240.40	53.79
ELAISN1_11	DIS	16	242.82	52.90
ELAISN1_12	DIS	12	244.11	54.00
ELAISN2_00	DIS	27	249.21	41.04
ELAISN2_01	DIS	14	247.82	41.07
ELAISN2_03	DIS	15	250.54	41.37
ELAISN2_04	DIS	15	250.15	40.27
ELAISN2_05	DIS	11	248.55	40.05
ELAISN2_06	DIS	11	248.20	41.47
ELAISN2_07	DIS	12	248.75	40.28
ELAISN2_08	DIS	12	249.67	41.90
ELAISS1_00	DIS	31	9.64	-43.99
ELAISS1_01	DIS	21	9.32	-42.97
ELAISS1_02	DIS	37	11.08	-43.85
ELAISS1_03	DIS	32	10.40	-44.89
ELAISS1_04	DIS	32	8.92	-44.91
ELAISS1_05	DIS	47	7.66	-44.35
ELAISS1_08	DIS	29	7.70	-42.82
ELAISS1_11	DIS	46	9.12	-41.73
ELAISS1_15	DIS	27	8.84	-43.80
G11_005001_J000211m430725	G11	11	0.55	-43.12

Table 1—Continued

Field	Survey	Visits	Right Ascension	Declination
G11_005007_J092810p702308	GII	22	142.04	70.39
G11_005008_J100924p280300	GII	15	152.35	28.05
G11_005015_J132648p660300	GII	17	201.70	66.05
G11_005021_J154712m131514	GII	42	236.80	-13.25
G11_013007_IRASF09111m1007	GII	16	138.41	-10.32
G11_013023_IRASF10038m3338	GII	11	151.52	-34.14
G11_014001_NGC2442	GII	15	113.50	-69.80
G11_022001_CL0024p1654	GII	14	6.65	17.16
G11_022002_MS0451m0301	GII	90	73.43	-2.62
G11_024002_DEEP_IMPACT	GII	10	204.47	-9.56
G11_032001_NGC5291	GII	17	206.94	-30.45
G11_035001_J104802p052610	GII	63	162.01	5.44
G11_035002_J105002p042644	GII	53	162.51	4.45
G11_036037_NGC6574	GII	11	272.96	14.98
G11_041001_EF_ERI	GII	21	48.55	-22.59
G11_041002_SDSS155331p5516	GII	22	238.50	55.44
G11_043001_AE_AQR	GII	31	310.04	-0.87
G11_045001_AM1806m852	GII	20	279.32	-85.40
G11_045007_AM1434m783	GII	20	220.12	-78.64
G11_052002_KIG557	GII	13	193.82	0.25
G11_052004_KIG792	GII	40	257.96	18.84
G11_056009_NGC2298	GII	17	102.07	-35.94
G11_056023_NGC6218	GII	19	251.81	-1.95
G11_056025_NGC6235	GII	31	253.37	-22.59
G11_056026_NGC6254	GII	18	254.29	-4.10
G11_056028_Pal_11	GII	15	296.43	-7.94
G11_059003_NGC2865	GII	14	140.88	-23.16
G11_061002_NGC0300	GII	10	13.72	-37.68
G11_065001_SubaruDeep	GII	71	201.09	27.49
G11_071001_M81	GII	20	148.69	69.19
G11_073009_J231524p185859	GII	19	348.85	18.98
G11_074001_J120526m074324	GII	54	181.36	-7.72
G11_098001_A0426	GII	15	49.90	41.50
G11_113003_V476_CYG	GII	11	299.60	53.62
G11_114001_RXJ0122m7521	GII	36	20.72	-75.35
G11_114003_PG11159m035	GII	24	180.44	-3.76
G11_114004_PG0038p199	GII	14	10.40	20.15
G12_001001_HYADES_POS1	GII	14	68.57	17.15
G12_001002_HYADES_POS2	GII	12	66.95	17.09
G12_007006_S_121410p140127	GII	24	183.54	14.02
G12_007011_S_141753p251014	GII	33	214.47	25.17
G12_007012_S_143907p641712	GII	19	219.78	64.29
G12_046001_COMA3	GII	27	194.34	27.18
G12_057001_NGC55	GII	28	3.79	-39.22
GROTH_00	DIS	187	214.99	52.78
HDFN_00	DIS	103	189.21	62.20
LOCK_00	DIS	46	162.68	58.73
LOCK_01	DIS	22	160.70	58.52
LOCK_02	DIS	25	161.02	59.45
LOCK_03	DIS	24	159.00	59.21
LOCK_04	DIS	23	161.75	57.90
LOCK_05	DIS	63	163.29	56.95
LOCK_06	DIS	21	158.83	58.13
LOCK_07	DIS	28	164.19	58.27
LOCK_08	DIS	17	160.01	56.60
LOCK_09	DIS	25	163.23	59.78
LOCK_10	DIS	21	161.45	55.97
LOCK_11	DIS	28	165.00	59.19
LOCK_12	DIS	24	159.52	57.76
LOCK_13	DIS	24	157.35	57.42
LOCK_15	DIS	21	163.09	57.88
LOCK_18	DIS	10	161.40	56.36
LOCK_19	DIS	11	163.20	59.20
MSJ2137	DIS	33	325.12	-23.94
NGA_Cen_A_Jet	NGS	18	201.80	-42.90
NGPDWS_00	DIS	76	219.16	35.17

Table 1—Continued

Field	Survey	Visits	Right Ascension	Declination
NGPDWS_01	DIS	15	217.86	35.41
NGPDWS_03	DIS	10	218.15	34.60
NGPDWS_04	DIS	12	216.55	35.45
NGPDWS_15	DIS	12	216.40	34.35
NSC_J171150p160145	DIS	12	257.96	16.03
PHOENIX_00	DIS	12	17.70	-45.75
QSOHE2347	DIS	24	357.64	-43.43
SIRTFFL_00	DIS	28	259.12	59.91
SIRTFFL_01	DIS	20	260.41	59.34
SIRTFFL_02	DIS	10	260.11	58.50
SIRTFFL_03	DIS	11	258.33	58.87
UVE_A0216	DIS	10	24.20	-6.38
UVE_A0389	DIS	23	42.88	-24.93
UVE_A0951	DIS	35	153.38	34.62
UVE_A1643	DIS	11	193.98	44.29
UVE_A1979	DIS	24	222.75	31.28
UVE_A2048	DIS	19	228.82	4.38
UVE_A2235	DIS	55	253.74	39.52
UVE_A2670	DIS	10	358.54	-10.41
UVE_A3330	DIS	48	79.18	-49.07
UVE_FORNAX	DIS	12	54.10	-35.55
VIRGOHI21	DIS	25	184.85	14.60
VVDS22H	DIS	54	334.43	0.67
WHTDF_00	DIS	24	5.65	0.36
WIRE_0813p02	DIS	77	123.51	3.49
XMMLSS_00	DIS	49	36.66	-4.48
XMMLSS_01	DIS	70	36.36	-4.48
XMMLSS_02	DIS	15	36.58	-5.51
XMMLSS_03	DIS	19	35.47	-5.52
XMMLSS_04	DIS	16	34.91	-5.10
XMMLSS_05	DIS	17	36.48	-3.60
XMMLSS_06	DIS	20	34.60	-3.65
XMMLSS_07	DIS	20	34.10	-5.83
XMMLSS_08	DIS	17	35.06	-6.30
XMMLSS_09	DIS	20	34.12	-4.64
XMMLSS_12	DIS	18	33.66	-3.68
XMMLSS_20	DIS	18	35.65	-4.65

Table 2. The GALEX Ultraviolet Variability Catalog

GALEX	SDSS or USNO-B1	SIMBAD	Type	Field	N_{det}	NUV_{max}	Δm	N_{det}	FUV_{max}	Δm	g or B	r or R	i or I
J001437.6-392632.2	0505-0002317			GI2_057001_NGC55	19	19.38	0.70	0	-	-	18.22	17.46	18.09
J001530.6-384855.9	0511-0002596			GI2_057001_NGC55	19	19.02	1.72	6	20.34	3.45	15.86	13.87	13.39
J001611.6-392721.5	0505-0002614			GI2_057001_NGC55	19	16.16	2.02	16	17.59	5.81	14.91	13.75	13.95
J002147.4+000031.3	J002147.52+000030.9	RX J0021.7+0000	X	WHTDF_00	24	20.18	0.67	24	20.16	1.07	19.58	19.18	18.28
J002442.4+165808.0	1069-0004486			GI1_022001_CL0024p1654	8	17.68	0.71	1	22.79	-	13.62	13.03	12.67
J002904.4-425242.9	0471-0004614	ELAISC15 J002904-425243	QSO	ELAISS1_08	26	19.88	0.92	22	20.66	1.86	20.00	19.43	18.54
J002906.7-423904.2	0473-0006317			ELAISS1_08	29	18.40	0.66	24	18.96	0.93	19.78	19.05	18.74
J003017.4-422446.3	0475-0007085	QSO B0027-426	QSO	ELAISS1_08	16	18.07	0.63	11	18.54	0.96	19.13	18.26	18.49
J003043.0-422747.7	0475-0007155			ELAISS1_08	29	17.25	1.48	18	19.92	3.73	15.84	14.53	14.44
J003215.4-425344.3	0471-0005077			ELAISS1_08	29	20.08	0.75	24	20.74	1.62	19.56	20.03	-
J003301.7-440750.8	0458-0004766	ELAISC15 J003301-440748	QSO	ELAISS1_15	68	19.62	0.73	55	20.28	1.33	20.13	19.51	18.76
J003331.3-441039.1	0458-0004818			ELAISS1_15	27	19.81	1.17	23	20.54	2.12	19.60	19.71	18.64
J003336.5-434914.2	0461-0005149	SV* BV 983	V*	ELAISS1_15	24	14.75	0.75	24	19.57	1.07	11.50	11.05	10.87
J003358.8-435741.7	0460-0005106	ELAISC15 J003358-435739		ELAISS1_15	27	18.30	2.12	3	20.44	0.24	12.67	11.26	11.43
J003454.2-444617.1	0452-0004745			ELAISS1_04	17	20.28	0.68	16	20.67	1.03	20.37	19.38	18.74
J003459.3-444928.9	0451-0005029			ELAISS1_04	31	19.30	1.05	26	19.48	1.22	19.79	19.00	18.76
J003536.9-443104.5	0454-0004871			ELAISS1_04	30	20.18	0.81	25	21.34	1.73	20.44	19.45	-
J003544.1-451818.6	0446-0005285			ELAISS1_04	31	19.72	0.63	26	20.68	0.90	20.26	19.38	18.71
J003632.2-451014.2	0448-0005207			ELAISS1_04	31	20.01	0.81	0	-	-	20.24	19.14	18.67
J003753.0-432824.7	0465-0005598			ELAISS1_00	48	18.88	0.76	47	19.10	1.09	19.66	19.26	18.76
J003809.4-435241.1	0461-0005747			ELAISS1_00	54	19.32	0.78	53	19.97	1.27	20.72	19.57	18.76
J003900.2-445721.5	0450-0005466			ELAISS1_03	29	18.83	0.75	25	19.64	1.32	19.56	18.90	18.74
J003938.5-450942.5	0448-0005594			ELAISS1_03	32	19.85	0.78	28	20.10	0.88	20.07	19.10	18.75
J004033.8-445936.9	0450-0005656			ELAISS1_03	32	20.14	0.78	0	-	-	-	19.78	18.49
J004047.4-434948.8	0461-0006186			ELAISS1_00	24	18.20	1.95	9	19.80	4.13	17.25	16.27	15.89
J004215.3+200957.3	1101-0008473			GI1_114004_PG0038p199	15	18.94	1.65	1	21.30	-	13.88	12.35	11.08
J004320.9-445322.8	0451-0006311			ELAISS1_03	32	19.61	0.68	25	22.05	1.11	-	19.64	18.31
J004347.7-445130.7	0451-0006391			ELAISS1_03	23	16.78	0.84	22	19.11	2.00	15.87	15.17	15.75
J011010.9-452431.3	0445-0009414			PHOENIX_00	11	18.84	1.85	2	21.45	1.26	17.88	17.15	18.64
J011050.4-460013.8	0439-0009514	LEHPM 1305		PHOENIX_00	10	19.33	1.59	6	20.65	1.85	-	13.87	17.56
J011805.2-751126.1	0148-0012155	V* BG Tuc	RR*	GI1_114001_RXJ0122m7521	14	18.61	1.41	3	20.82	1.75	17.59	16.52	15.51
J012123.4-755149.5	0141-0008485			GI1_114001_RXJ0122m7521	14	20.01	0.97	2	23.20	0.25	18.13	17.38	17.47
J012151.7-745125.2	0151-0015590			GI1_114001_RXJ0122m7521	13	20.27	0.60	5	22.22	0.73	18.71	17.12	16.94
J013642.0-062743.1	0835-0014625			UVE_A0216	10	19.70	0.63	0	-	-	16.79	16.31	16.12
J021547.1-045207.8	0851-0021482			XMMMLSS_09	7	19.60	0.67	1	23.56	-	15.06	12.96	12.37
J021551.8-061733.2	0837-0021646			XMMMLSS_07	8	19.73	0.81	8	21.10	1.50	20.65	19.89	18.92
J021632.0-061215.0	0837-0021759			XMMMLSS_07	8	20.06	0.61	1	23.68	-	20.65	20.21	18.93
J021731.7-040140.2	0859-0021367			XMMMLSS_06	7	19.78	0.78	7	20.59	1.29	-	-	-
J021820.4-050425.6	0849-0021282			XMMMLSS_04	2	20.25	0.74	2	21.20	1.48	18.85	18.94	18.85
J022003.0-032910.7	0865-0022411			XMMMLSS_06	7	20.01	0.73	0	-	-	16.19	14.44	13.77
J022003.0-035247.0	0861-0022258			XMMMLSS_06	6	19.85	0.76	6	21.28	1.28	20.69	20.63	-
J022050.6-061528.0	0837-0022491			XMMMLSS_08	7	18.99	0.77	3	21.47	2.43	14.67	13.14	12.24
J022128.7-055857.1	0840-0022257			XMMMLSS_03	7	20.07	0.83	7	20.57	1.47	20.31	20.28	18.94
J022258.8-045851.9	0850-0022815			XMMMLSS_20	7	20.19	0.70	7	20.60	0.84	20.24	19.77	18.84
J022424.1-043229.8	0854-0022429	XMDS J022424.1-043228	X	XMMMLSS_01	29	20.09	0.77	19	22.05	1.67	20.02	20.11	-
J022438.9-042706.0	0855-0022677	PMUKS (BJ) B022208.33-044038.	AGN	XMMMLSS_01	13	19.76	0.75	13	19.78	0.89	19.06	17.09	16.83
J022521.8-050017.4	0849-0022409			XMMMLSS_01	11	19.42	1.57	4	20.69	2.67	18.56	17.37	17.20
J022607.7-041843.0	0856-0023092	XMDS J022607.7-041843	X	XMMMLSS_01	00	19.71	0.68	84	20.11	1.17	19.80	20.37	18.71
J025122.8-244738.1	0652-0031877			UVE_A0389	24	19.44	0.68	16	19.30	0.95	16.82	15.70	15.28
J031229.6-224710.3	0672-0049382			GI1_041001_EF_ERI	12	20.00	0.90	2	23.54	0.01	15.53	13.79	13.11

Table 2—Continued

GALEX	SDSS or USNO-B1	SIMBAD	Type	Field	N_{det}	NUV_{max}	Δm	N_{det}	FUV_{max}	Δm	g or B	r or R	i or I
J032954.9-290801.4	0608-0035340			CDFS_07	6	19.44	0.62	0	-	-	16.05	15.19	15.14
J033030.6-292925.0	0605-0036442			CDFS_08	18	19.67	1.08	17	20.29	0.84	18.09	17.33	17.87
J033147.9-263142.0	0634-0055190	2MASS J03314795-2631415		CDFS_02	8	20.05	0.90	5	23.18	0.45	15.09	12.68	12.72
J033202.0-270251.0	0629-0052136			CDFS_10	24	18.68	0.69	24	20.28	1.87	13.40	11.55	11.36
J033339.3-281723.6	0617-0035918			CDFS_00	37	19.65	0.81	37	20.73	1.16	19.99	19.72	-
J033427.8-271222.3	0627-0053059			CDFS_03	24	17.92	1.71	7	20.76	2.56	16.68	15.08	14.98
J033438.6-352904.2	0545-0029296			UVE_FORNAX	12	18.60	1.12	11	20.54	2.31	12.89	11.37	10.58
J033500.4-272854.8	0625-0053892	BPS CS 29526-0042		CDFS_03	27	16.98	1.63	16	19.37	4.07	14.74	14.27	13.99
J033502.7-271210.1	0627-0053178			CDFS_03	26	19.98	0.90	24	20.80	1.51	19.97	18.84	18.66
J033546.0-290209.8	0609-0037329	HE 0333-2912		CDFS_09	10	16.09	0.90	10	18.10	2.61	13.39	13.42	13.14
J033621.1-353335.3	0544-0029832	[MDP2001] 18	QSO	UVE_FORNAX	11	20.24	0.74	11	21.00	1.27	19.27	20.05	-
J033621.6-270700.3	0628-0052915			CDFS_03	22	20.32	0.67	22	21.49	1.21	19.88	18.16	-
J033715.2-283238.1	0614-0037520	2MASS J03371533-2832382		CDFS_09	12	15.51	0.94	12	16.78	3.07	13.88	13.52	13.23
J033721.8-271636.5	0627-0053616			CDFS_03	10	20.33	0.67	8	22.48	0.53	19.74	18.90	-
J033728.9-354108.5	0543-0030374	[MDP2001] 3	QSO	UVE_FORNAX	11	20.05	0.94	11	20.37	1.44	18.60	19.16	18.47
J033808.7-353418.9	0544-0030090	[PFP2002] 19	X	UVE_FORNAX	8	20.24	0.72	6	22.53	0.65	14.47	12.86	11.46
J033818.4-272232.8	0626-0054340			CDFS_03	2	19.39	1.15	2	20.28	1.80	17.13	14.51	12.60
J033825.1-273326.6	0624-0054706			CDFS_03	12	20.17	0.71	12	21.25	1.30	20.05	19.54	18.71
J033843.5-353349.1	0544-0030186	[MCJ93] NGC 1404 a	QSO	UVE_FORNAX	10	20.16	0.60	9	21.24	1.05	18.72	19.48	18.74
J042733.6+165222.2	1068-0045716	Cl* Melotte 25 LH 110		GI2_001002_HYADES_POS2	5	20.18	0.73	5	21.38	0.79	16.34	14.90	12.93
J042832.3+165821.6	1069-0046050			GI2_001002_HYADES_POS2	7	19.30	1.64	1	20.74	-	16.60	15.96	14.90
J043431.2+172220.1	1073-0063497			GI2_001001_HYADES_POS1	13	19.66	0.71	13	20.47	0.31	17.23	15.05	14.36
J051358.9-481609.7	0417-0042965			DLENSS_02	9	19.59	1.31	0	-	-	12.23	11.09	10.62
J051439.0-491136.9	0408-0043566			DLENSS_00	49	19.30	1.46	2	23.53	0.16	16.57	15.03	15.02
J051456.0-485234.5	0411-0043202	1RXS J051455.4-485238	X	DLENSS_00	47	20.25	0.74	14	21.12	1.22	-	18.52	18.27
J051507.4-485739.4	0410-0042890			DLENSS_00	40	19.78	0.70	23	20.61	0.73	18.87	19.43	-
J051522.4-494528.8	0402-0043026			DLENSS_05	19	17.15	0.69	17	22.60	0.80	13.82	13.78	13.12
J051544.9-484853.6	0411-0043441			DLENSS_00	65	19.83	0.69	28	20.42	1.32	20.35	20.15	18.67
J051630.7-484850.5	0411-0043607			DLENSS_02	49	19.29	1.70	12	21.40	2.18	17.91	16.37	16.79
J051633.9-475139.5	0421-0054904			DLENSS_02	11	19.88	0.62	6	21.61	1.67	18.58	18.27	18.02
J051659.7-485211.9	0411-0043744	HD 273973		DLENSS_00	69	15.46	1.05	31	20.09	1.04	12.48	12.41	12.39
J051728.7-481712.8	0417-0043781			DLENSS_02	6	18.60	1.42	3	21.24	1.62	16.87	15.89	15.59
J051822.2-484151.8	0413-0044067			DLENSS_02	59	19.13	1.12	34	19.75	1.13	20.18	19.44	18.85
J051828.9-483932.8	0413-0044092			DLENSS_02	32	19.50	1.50	26	19.32	1.77	18.46	17.16	16.62
J051832.6-484541.1	0412-0043599			DLENSS_02	65	19.56	0.87	28	20.04	1.39	19.42	19.20	18.69
J051841.6-490713.4	0408-0044496	1RXS J051841.2-490711	X	DLENSS_00	9	20.25	0.75	6	22.04	1.07	15.56	13.14	12.53
J051855.0-492606.1	0405-0044152			DLENSS_05	11	17.59	0.84	7	19.99	2.50	15.38	14.82	14.78
J052147.9-485240.8	0411-0044640			DLENSS_03	34	20.18	0.69	34	20.39	1.00	21.16	20.13	-
J052307.7-490336.1	0409-0043999			DLENSS_03	20	18.17	2.13	6	19.58	3.58	16.74	15.94	15.54
J052337.8-485917.4	0410-0044641			DLENSS_03	37	18.81	1.26	0	-	-	14.43	13.31	13.26
J052343.6-481357.0	0417-0045213			DLENSS_01	14	19.85	0.98	14	20.14	1.11	19.19	18.93	18.20
J064620.4-361255.1	0537-0071696			GI1_056009_NGC2298	3	19.65	0.76	0	-	-	14.15	13.03	12.86
J064656.0-361528.9	0537-0071933			GI1_056009_NGC2298	19	18.21	2.66	0	-	-	12.28	11.77	11.56
J064753.2-353947.6	0543-0073588			GI1_056009_NGC2298	21	20.00	1.00	0	-	-	16.34	14.88	14.31
J064818.6-362115.6	0536-0071322			GI1_056009_NGC2298	25	19.22	0.85	0	-	-	13.55	12.94	12.56
J064856.6-360215.8	0539-0072748			GI1_056009_NGC2298	2	19.67	0.62	1	18.58	-	17.60	16.41	16.58
J065023.1-354827.2	0541-0073790			GI1_056009_NGC2298	2	19.05	1.63	1	22.16	-	15.07	13.38	11.45
J081226.4+033320.5	J081226.37+033320.1			WIRE_0813p02	77	18.95	1.95	0	-	-	16.68	16.49	16.43
J090853.4-021242.8	0877-0274765			EIS_WIDE_D	13	19.23	0.98	9	22.69	0.85	15.90	15.66	16.16
J091215.2-101203.7	0797-0189197			GI1_013007_IRASF09111m1007	11	18.98	1.94	2	19.54	3.22	16.40	15.84	14.56

Table 2—Continued

GALEX	SDSS or USNO-B1	SIMBAD	Type	Field	N_{det}	NUV_{max}	Δm	N_{det}	FUV_{max}	Δm	g or B	r or R	i or I
J091303.9-095637.5	0800-0190480			G11_013007_IRASF09111m1007	3	17.93	3.02	0	-	-	16.72	16.51	15.50
J091332.6-101108.2	0798-0190682			G11_013007_IRASF09111m1007	15	19.11	1.47	3	19.27	0.28	15.35	14.15	13.46
J092251.4-230407.1	0669-0247513			G11_059003_NGC2865	11	17.71	2.00	0	-	-	14.97	15.17	14.65
J092538.3-225707.7	0670-0257587			G11_059003_NGC2865	9	20.00	0.70	2	21.06	0.32	16.84	16.29	16.12
J093251.3+700152.7	1600-0086111			G11_005007_J092810p702308	19	20.32	0.66	9	20.93	0.24	19.81	18.80	18.37
J095819.9+022903.6	J095819.87+022903.5	SDSS J095819.87+022903.5	Sy1	COSMOS_03	56	19.12	0.61	50	19.38	0.78	19.36	19.14	19.09
J095820.4+020303.9	J095820.44+020303.9	SDSS J095820.44+020303.9	QSO	COSMOS_03	16	20.35	0.64	12	23.05	1.33	20.05	19.86	19.83
J095821.6+024628.2	J095821.65+024628.1	SDSS J095821.65+024628.1	QSO	COSMOS_03	47	20.39	0.61	9	22.77	1.53	19.53	19.20	19.08
J095847.6+021815.3	J095847.63+021814.9			COSMOS_03	11	18.62	1.42	1	23.43	-	14.56	13.78	13.68
J095848.7+025243.9	J095848.67+025243.2	2MASX J09584864+0252433	Sy1	COSMOS_03	37	20.11	0.85	31	20.91	0.60	18.96	17.99	17.67
J095902.7+021906.5	J095902.76+021906.3	2MASS J09590277+0219067	QSO	COSMOS_03	01	19.80	0.64	91	20.25	0.89	19.66	19.10	18.92
J100015.7+025545.4	J100015.76+025545.5	[VV2006c] J100015.7+025545	Sy1	COSMOS_03	49	20.14	0.85	45	20.47	1.19	19.11	18.40	17.97
J100024.6+023149.1	J100024.64+023149.0	SDSS J100024.64+023149.0	QSO	COSMOS_03	12	19.24	0.97	54	22.64	1.65	19.14	18.89	18.93
J100133.2+014328.5	J100133.25+014328.5			COSMOS_02	56	17.21	1.98	24	18.93	5.79	14.69	14.66	14.68
J100146.5+020256.7	J100146.48+020256.7			COSMOS_01	03	20.14	0.62	93	20.59	1.08	20.21	20.19	20.17
J100152.2+021158.7	0921-0232199			COSMOS_01	72	19.17	1.31	62	21.10	2.30	14.34	12.58	11.91
J100202.8+022433.9	J100202.77+022434.6	SDSS J100202.77+022434.6	QSO	COSMOS_01	82	20.30	0.64	35	23.03	1.18	20.31	20.11	20.33
J100317.9+022356.3	J100317.92+022355.6			COSMOS_01	20	20.37	0.60	17	22.07	1.61	20.57	20.45	20.30
J100614.4-340233.1	0559-0228154			G11_013023_IRASF10038m3338	6	19.46	0.80	0	-	-	14.52	13.53	12.90
J100856.4+280008.1	J100856.40+280008.2			G11_005008_J100924p280300	15	19.75	0.72	13	21.01	0.49	19.47	19.62	19.45
J102641.8+572858.7	J102641.84+572858.4			LOCK_13	23	18.78	1.84	3	22.13	1.62	16.90	16.51	16.41
J102841.9+570840.4	1471-0248108			LOCK_13	24	18.27	1.26	2	22.48	1.08	14.00	12.85	12.49
J102911.8+575806.1	1479-0255037	TYC 3822-603-1		LOCK_13	18	19.54	1.13	8	21.67	1.08	11.52	9.78	8.96
J103222.8+575551.8	J103222.85+575551.1	CLASXS 89	QSO	LOCK_06	18	20.05	0.69	10	20.77	0.58	20.19	19.96	20.04
J103333.9+582818.8	J103333.92+582818.8	SDSS J103333.92+582818.8	QSO	LOCK_06	20	20.19	0.75	10	20.92	1.03	20.31	20.42	20.22
J103352.8+584655.1	J103352.86+584654.7	V* DW UMa	Nov	LOCK_03	23	15.17	0.65	11	15.21	0.65	14.33	14.33	14.35
J103402.9+582639.7	J103402.86+582639.6			PQ	19	20.36	0.63	10	20.74	0.54	19.87	19.77	19.47
J103525.0+580336.1	J103525.05+580335.6	SDSS J103525.05+580335.6	QSO	LOCK_12	43	19.52	0.71	19	20.60	0.63	19.05	18.95	19.06
J103538.2+581549.1	1482-0238267			LOCK_06	20	15.53	1.92	10	16.78	5.68	13.59	12.96	12.24
J103557.6+591934.8	J103557.67+591934.3			LOCK_03	24	17.98	0.90	11	18.22	1.02	18.02	18.13	18.08
J103607.2+592251.3	1493-0195709			LOCK_03	6	20.18	0.80	2	21.26	0.03	14.47	13.52	14.23
J103653.0+584734.9	J103653.00+584734.2	SDSS J103653.00+584734.2	QSO	LOCK_03	18	19.82	0.65	7	21.18	0.47	20.22	19.69	19.69
J103717.0+563456.9	J103716.99+563456.9	SDSS J103716.99+563456.9	QSO	LOCK_08	21	19.16	0.68	10	19.82	0.94	19.09	18.90	18.94
J103720.9+591653.8	J103720.93+591653.5			LOCK_03	24	18.31	0.62	11	20.50	1.77	16.05	16.02	16.03
J103735.2+563050.6	J103735.17+563050.7			PQ	20	19.74	0.76	9	20.51	1.13	19.49	19.39	19.50
J103755.2+575512.2	J103755.23+575512.0	1RXS J103755.6+575514	X	LOCK_12	34	19.97	0.61	17	20.73	0.90	19.84	19.60	19.62
J103759.4+581213.5	J103759.47+581212.7			LOCK_12	35	19.67	1.03	5	22.84	1.02	17.34	17.22	17.17
J103918.8+561101.6	J103918.78+561101.6	SDSS J103918.78+561101.6	QSO	LOCK_08	21	20.27	0.63	10	21.30	0.91	19.16	19.06	18.85
J104013.0+564141.1	J104013.31+564140.9			LOCK_08	20	19.63	0.61	9	20.19	0.56	20.07	20.11	19.74
J104017.0+565829.7	J104017.02+565828.9			PQ	21	19.78	1.03	10	20.70	1.23	19.57	19.61	19.65
J104100.0+564713.7	J104100.00+564713.3	SDSS J104100.00+564713.3	QSO	LOCK_08	21	19.59	0.81	0	-	-	18.16	18.12	18.10
J104108.2+562000.3	J104108.18+562000.3	2MASS J10410822+5620002	AGN	LOCK_08	18	20.04	0.94	9	19.50	0.57	19.82	18.78	18.43
J104114.4+575024.1	J104114.48+575023.9	SDSS J104114.48+575023.9	QSO	LOCK_12	24	20.07	0.71	11	20.38	0.82	18.84	18.89	18.71
J104325.0+563258.0	J104325.06+563258.1			LOCK_08	26	16.40	3.74	18	17.78	2.41	20.28	20.40	20.58
J104350.5+553921.0	J104350.48+553921.0			LOCK_10	20	20.02	0.73	8	22.86	0.78	20.10	19.95	20.01
J104356.6+580732.1	J104356.72+580731.9	V* IY UMa	Nov	LOCK_01	29	17.59	0.94	12	17.97	0.81	17.52	17.62	17.60
J104401.1+560003.4	J104401.13+560003.6	PQ	Nov	LOCK_10	15	20.25	0.71	11	20.90	1.07	20.26	20.01	19.99
J104537.4+594656.1	J104537.46+594655.6	1RXS J104537.1+594648	X	LOCK_02	24	19.25	1.29	12	22.08	1.11	14.27	13.45	12.92
J104551.8+562206.9	J104551.80+562203.5	SDSS J104551.80+562203.5	QSO	LOCK_10	39	18.97	1.44	20	20.33	0.86	18.94	18.74	18.69
J104640.7+590522.0	J104640.55+590524.2			LOCK_02	9	20.21	0.74	2	20.99	0.25	20.49	20.25	19.92

Table 2—Continued

GALEX	SDSS or <i>USNO-B1</i>	SIMBAD	Type	Field	N_{det}	NUV_{max}	Δm	N_{det}	FUV_{max}	Δm	g or B	r or R	i or I
J132733.1-430701.1	<i>0468-0336855</i>			NGA_Cen_A_Jet	8	20.17	0.81	0	-	-	<i>17.24</i>	<i>17.44</i>	<i>17.60</i>
J132743.5+654652.2	J132743.54+654651.9	SDSS J132743.54+654651.9	Sy1	G11_005015_J132648p660300	6	20.11	0.87	4	21.77	0.26	19.95	20.08	19.73
J132755.7-424752.2	<i>0472-0378078</i>			NGA_Cen_A_Jet	7	20.19	0.78	1	22.95	-	<i>16.57</i>	<i>16.82</i>	<i>16.49</i>
J132832.4-424144.0	<i>0473-0382414</i>	2E 3056	X	NGA_Cen_A_Jet	6	20.32	0.64	1	22.57	-	<i>15.08</i>	<i>12.70</i>	<i>11.23</i>
J133922.6-092349.4	<i>0806-0257175</i>			G11_024002_DEEP_IMPACT	7	19.81	1.02	0	-	-	<i>19.45</i>	<i>18.81</i>	<i>18.27</i>
J134651.1-300451.8	<i>0599-0303916</i>			G11_032001_NGC5291	7	19.62	1.37	0	-	-	<i>17.59</i>	<i>16.47</i>	<i>16.64</i>
J134939.3-301623.8	<i>0597-0305628</i>	[RP98d] P12	QSO	G11_032001_NGC5291	9	19.62	1.06	0	-	-	<i>18.61</i>	<i>18.44</i>	<i>18.12</i>
J141724.6+523025.1	J141724.59+523024.9	CFDF 14h 50800	Sy1	GROTH_00	84	20.36	0.64	35	20.98	0.75	20.17	20.04	19.73
J141801.5+525200.9	J141801.51+525200.7		PQ	GROTH_00	45	20.32	0.67	63	21.07	1.19	20.45	20.18	20.13
J141818.9+525007.2	<i>1428-0298757</i>	2MASS J14181898+5250068	**	GROTH_00	53	17.68	0.69	54	22.36	1.91	<i>13.55</i>	<i>12.24</i>	<i>12.06</i>
J141905.1+522528.2	J141905.17+522527.7	SDSS J141905.17+522527.7	QSO	GROTH_00	53	20.17	0.83	77	20.97	1.30	19.95	19.88	19.69
J141949.6+530555.0	J141949.62+530554.7			GROTH_00	66	19.66	0.67	68	21.63	2.50	17.75	17.69	17.71
J142015.6+523718.9	J142015.64+523718.8	SDSS J142015.64+523718.8	QSO	GROTH_00	68	20.16	0.79	77	21.08	0.63	19.28	19.26	19.10
J142023.9+531605.2	J142023.88+531605.0			GROTH_00	63	20.30	0.70	23	21.25	1.98	20.70	20.63	20.63
J142135.9+523139.2	J142135.88+523138.9	HSP2005] J142135.894+523137.8	Gal	GROTH_00	02	19.91	0.79	48	20.03	0.84	19.84	19.23	18.87
J142209.1+530559.3	J142209.14+530559.7			GROTH_00	58	19.74	0.84	74	20.74	1.38	19.55	19.51	19.51
J142337.7+341053.1	J142337.63+341052.9	1RXS J142337.6+341049	X	NGPDWS_15	35	18.98	0.98	1	19.81	-	18.68	18.49	18.91
J142338.9+342242.8	J142338.89+342242.6			NGPDWS_15	36	19.18	0.81	0	-	-	18.44	18.21	18.13
J142456.4+341812.6	J142456.37+341812.4			NGPDWS_15	36	19.44	0.69	1	21.77	-	19.58	19.38	19.44
J142607.7+340426.4	J142607.71+340426.3	BWE 1423+3417	BLL	NGPDWS_15	35	18.93	0.90	1	21.97	-	17.65	17.38	17.12
J142627.0+321540.7	<i>1222-0300203</i>			NGPDWS_08	26	20.33	0.64	1	20.84	-	<i>19.25</i>	<i>18.40</i>	<i>18.69</i>
J142734.8+352543.1	J142734.80+352543.4	[VV2006c] J142734.8+352543	Sy1	NGPDWS_04	37	19.24	0.60	1	19.55	-	18.45	18.29	18.34
J142747.3+350344.4	J142747.26+350344.1			NGPDWS_04	53	20.32	0.66	0	-	-	20.25	19.95	19.83
J142808.4+320624.6	J142808.47+320624.7			NGPDWS_08	25	20.02	0.96	1	21.42	-	19.54	19.54	19.24
J142809.2+341342.0	J142809.21+341342.0			NGPDWS_15	59	19.11	1.05	2	20.30	0.04	19.43	19.57	19.28
J142909.9+353614.7	J142909.96+353615.0			NGPDWS_01	21	20.00	0.88	13	20.65	0.86	19.57	18.86	18.44
J142911.3+324824.2	J142911.27+324824.0			NGPDWS_13	21	18.88	0.65	1	20.14	-	18.17	17.99	17.98
J142924.2+353013.0	J142924.20+353013.0			NGPDWS_01	13	19.27	0.67	0	-	-	16.04	15.63	15.53
J142948.8+330839.0	J142948.72+330836.4			NGPDWS_13	42	19.74	0.78	0	-	-	18.39	17.48	17.03
J143012.5+343708.6	J143012.51+343708.6			NGPDWS_03	46	20.30	0.61	1	21.35	-	20.36	20.35	20.31
J143057.2+324441.6	J143057.20+324441.7	[ZEH2003] RX J1430.9+3244 1		NGPDWS_13	6	18.91	1.70	1	18.77	-	19.62	18.80	18.38
J143126.4+342710.3	<i>1244-0216520</i>			NGPDWS_03	30	18.40	0.86	0	-	-	<i>13.78</i>	<i>12.72</i>	<i>11.68</i>
J143126.8+352453.1	J143126.89+352453.3			NGPDWS_01	18	19.57	1.00	8	22.01	0.42	19.68	19.67	19.73
J143128.2+330702.4	J143128.23+330702.5			NGPDWS_13	23	20.24	0.67	1	21.44	-	19.58	19.36	19.43
J143130.2+343856.8	J143130.16+343857.5			NGPDWS_03	34	20.06	0.60	0	-	-	19.77	19.59	19.56
J143133.5+350601.6	J143133.53+350601.4			NGPDWS_01	20	20.19	0.63	8	22.16	0.70	19.47	19.34	19.22
J143147.0+344639.4	J143146.98+344640.0			NGPDWS_03	30	20.33	0.67	0	-	-	20.01	19.76	19.84
J143212.8+355534.9	J143212.84+355534.5			NGPDWS_01	20	19.72	0.66	12	21.27	0.91	19.46	19.39	19.59
J143215.1+350525.0	J143215.15+350524.9			NGPDWS_01	42	19.74	0.87	13	20.26	0.74	19.45	19.50	19.46
J143304.3+332603.4	J143304.37+332603.7			NGPDWS_12	20	20.13	0.77	1	21.21	-	20.31	19.91	19.97
J143332.4+342050.1	J143332.36+342049.8			NGPDWS_12	54	19.18	1.59	1	22.43	-	19.15	19.17	19.38
J143411.2+334015.6	J143411.23+334015.3			NGPDWS_12	28	20.33	0.61	1	22.43	-	19.51	19.48	19.11
J143447.1+341249.9	J143447.15+341249.8			NGPDWS_12	50	20.33	0.66	1	21.07	-	19.92	19.84	19.57
J143448.1-782739.3	<i>0115-0081579</i>			G11_045007_AM1434m783	7	20.11	0.82	0	-	-	<i>18.24</i>	<i>16.73</i>	<i>17.24</i>
J143450.5+352433.1	J143450.50+352433.0			NGPDWS_00	80	19.85	1.13	68	21.16	1.54	20.81	20.52	20.52
J143528.3+350432.7	J143528.34+350432.6			NGPDWS_00	90	20.17	0.67	79	21.08	1.34	20.35	20.04	20.07
J143626.7+350029.4	J143626.63+350029.7	[VV2006] J143626.6+350029	QSO	NGPDWS_00	86	19.79	0.65	76	20.76	0.58	19.15	18.97	18.96
J143714.7+352254.3	J143714.66+352254.3			NGPDWS_00	89	19.25	0.70	78	19.84	1.06	19.34	19.45	19.29
J143750.3-785847.0	<i>0110-0077231</i>			G11_045007_AM1434m783	8	18.21	1.48	0	-	-	<i>15.58</i>	<i>15.29</i>	<i>14.65</i>
J143753.7+345924.0	<i>1249-0218617</i>	NSVS 7762964	RR*	NGPDWS_00	79	15.90	1.74	68	18.53	4.61	<i>13.49</i>	<i>13.93</i>	<i>13.18</i>

Table 2—Continued

GALEX	SDSS or USNO-B1	SIMBAD	Type	Field	N_{det}	NUV_{max}	Δm	N_{det}	FUV_{max}	Δm	g or B	r or R	i or I
J143756.5+351937.1	J143756.46+351937.0	7C 1435+3532	QSO	NGPDWS_00	80	18.17	0.92	78	18.93	1.04	18.36	18.58	18.39
J143805.6+345849.4	J143805.61+345849.4			NGPDWS_00	90	19.23	0.70	79	19.33	0.89	19.35	19.41	19.14
J143809.9+344604.7	J143809.84+344604.7			NGPDWS_00	66	20.02	0.61	60	20.71	1.37	20.17	20.14	20.29
J143813.0+344417.3	<i>1247-0218163</i>			NGPDWS_00	72	20.03	0.97	59	20.11	1.39	20.15	19.28	18.55
J143823.9+635329.9	J143823.99+635329.6			GI2-007012_S-143907p641712	11	19.23	0.76	4	22.11	1.28	16.80	16.63	16.60
J144033.3-781914.6	<i>0116-0085840</i>	NSV 6738	V*	GI1-045007_AM1434m783	6	17.09	0.79	0	-	-	14.25	14.24	13.91
J144153.9-784630.7	<i>0112-0079658</i>			GI1-045007_AM1434m783	8	19.84	1.10	0	-	-	14.34	12.81	12.34
J144227.8+643058.7	<i>1545-0184124</i>			GI2-007012_S-143907p641712	13	17.96	0.71	3	22.80	0.88	14.89	13.97	13.24
J145110.3+310639.8	<i>1211-0222759</i>	G 166-49		UVE_A1979	24	18.72	0.86	12	19.99	0.93	13.58	11.24	9.78
J151540.5+043032.0	J151540.50+043032.0	SDSS J151540.50+043032.0	QSO	UVE_A2048	9	20.35	0.61	8	21.43	0.92	19.69	19.53	19.21
J154550.8-124936.8	<i>0771-0380932</i>			GI1-005021_J154712m131514	25	19.51	0.62	0	-	-	16.08	16.13	16.23
J154603.5-125117.5	<i>0771-0381016</i>			GI1-005021_J154712m131514	27	19.89	0.67	0	-	-	18.40	19.72	18.81
J154636.0-125616.2	<i>0770-0374013</i>			GI1-005021_J154712m131514	27	20.03	0.69	0	-	-	15.96	15.50	15.13
J154756.8-130511.8	<i>0769-0363452</i>			GI1-005021_J154712m131514	27	17.82	1.54	0	-	-	15.32	14.79	14.27
J155800.6+535233.6	J155800.64+535233.6			ELAISN1_01	9	18.06	0.87	0	-	-	15.09	15.18	15.18
J160324.9+561258.4	J160324.93+561258.5			ELAISN1_06	3	19.54	1.05	0	-	-	17.48	17.31	17.32
J160451.2+543229.5	<i>1445-0249119</i>			ELAISN1_02	12	20.23	0.68	0	-	-	20.66	20.46	-
J160451.4+534311.4	<i>1437-0248184</i>			ELAISN1_09	16	19.14	1.07	2	22.85	0.51	13.91	12.89	11.84
J160538.0+561419.6	J160538.01+561419.5		PQ	ELAISN1_06	9	19.62	0.74	1	21.06	-	19.14	19.09	19.01
J160542.1+564848.5	J160542.07+564849.3			ELAISN1_06	2	20.12	0.79	0	-	-	17.35	17.18	17.18
J160551.1+554942.3	J160551.08+554942.8		PQ	ELAISN1_01	14	19.84	0.64	1	20.89	-	19.64	19.31	19.02
J160608.8+530519.0	J160608.91+530521.1			ELAISN1_09	12	18.76	1.53	0	-	-	13.89	13.60	13.46
J160655.4+534016.7	J160655.34+534016.8	SDSS J160655.34+534016.8	Sy1	ELAISN1_09	13	19.18	0.78	3	19.02	0.67	18.75	18.25	17.88
J160713.7+555132.0	J160713.78+555132.5			ELAISN1_01	14	18.80	1.30	0	-	-	15.45	15.50	15.57
J160730.2+560305.6	J160730.20+560305.5			ELAISN1_01	5	19.85	1.09	0	-	-	19.75	19.75	19.91
J160739.8+564243.2	J160739.66+564248.8			ELAISN1_06	2	20.22	0.74	0	-	-	15.46	15.05	14.92
J160752.0+552649.3	<i>1454-0249970</i>	TYC 3880-1282-1		ELAISN1_01	4	15.97	1.39	0	-	-	11.42	10.73	10.45
J160759.9+535209.9	J160759.92+535210.1			ELAISN1_09	12	19.20	0.90	2	22.84	0.13	16.83	16.84	16.82
J160809.7+554011.3	J160809.66+554011.4	RX J1608.1+5540	X	ELAISN1_01	4	20.09	0.82	1	20.17	-	19.81	19.42	18.97
J160857.9+524151.4	J160857.87+524151.3			ELAISN1_11	16	19.91	0.80	0	-	-	17.27	16.96	16.88
J160902.8+524224.4	J160902.80+524224.3		PQ	ELAISN1_11	18	19.11	0.74	3	19.75	0.78	17.37	17.52	17.67
J160939.2+563908.9	J160939.13+563909.4			ELAISN1_05	16	18.75	1.16	2	19.37	0.04	18.83	18.77	18.49
J161129.8+534346.2	J161129.86+534345.8			ELAISN1_04	13	18.20	1.98	0	-	-	16.52	16.19	16.10
J161212.5+540936.5	J161212.57+540936.6			ELAISN1_04	13	19.17	0.69	1	21.55	-	19.28	18.93	19.01
J161218.3+524225.4	<i>1427-0325138</i>			ELAISN1_11	17	18.33	1.58	1	20.03	-	13.90	12.85	11.43
J161238.8+564909.0	J161238.75+564909.7		PQ	ELAISN1_05	12	19.88	0.68	2	19.98	0.47	19.32	18.94	18.56
J161257.4+524103.1	J161257.41+524103.0			ELAISN1_11	19	19.48	1.06	4	20.00	0.43	19.72	19.66	19.39
J161405.2+534631.9	J161405.20+534631.8	1RXS J161405.6+534633	X	ELAISN1_04	14	20.14	0.84	1	20.35	-	19.16	18.90	18.83
J161502.9+563006.5	J161503.00+563006.8			ELAISN1_05	14	18.88	1.97	1	20.62	-	16.78	16.63	16.61
J161511.1+550625.8	J161511.06+550625.5		PQ	ELAISN1_00	14	18.98	0.67	12	19.37	0.21	18.64	18.81	18.69
J161618.1+545405.5	J161618.03+545406.1	1RXS J161618.8+545359	X	ELAISN1_00	22	19.87	0.88	0	-	-	19.80	19.38	19.39
J161705.4+551606.2	<i>1452-0248004</i>	V* CR Dra	FI*	ELAISN1_07	12	15.14	1.99	3	18.71	0.25	10.64	9.20	8.55
J163017.5+405425.5	J163017.46+405425.7			ELAISN2_01	14	18.45	1.21	0	-	-	15.52	15.57	15.60
J163117.8+411024.4	J163117.72+411024.1	2MASS J16311775+4110239	AGN	ELAISN2_01	5	20.32	0.61	1	21.43	-	19.88	19.18	18.86
J163118.7+405153.3	J163118.77+405152.1	2E 3717	X	ELAISN2_01	13	19.54	1.29	2	21.30	0.38	15.79	14.18	12.22
J163137.0+413656.3	J163137.06+413656.6			ELAISN2_06	18	20.22	0.62	0	-	-	19.56	19.53	19.28
J163143.7+404735.3	J163143.76+404735.6	SDSS J163143.76+404735.6	QSO	ELAISN2_01	13	19.96	0.67	2	20.53	0.36	19.16	18.99	18.71
J163146.7+414632.2	J163146.72+414632.6			ELAISN2_06	16	19.70	0.86	0	-	-	20.18	19.86	19.68
J163210.8+405502.8	J163210.88+405503.1	SDSS J163210.88+405503.1	QSO	ELAISN2_01	13	19.37	0.92	2	20.25	0.13	19.26	19.01	18.96
J163220.2+413836.5	J163220.16+413836.4			ELAISN2_06	2	20.05	0.72	0	-	-	19.99	19.73	19.84

Table 2—Continued

GALEX	SDSS or USNO-B1	SIMBAD	Type	Field	N_{det}	NUV_{max}	Δm	N_{det}	FUV_{max}	Δm	g or B	r or R	i or I
J163428.1+412742.7	J163428.13+412742.6			ELAISN2_06	6	19.89	1.09	0	-	-	20.63	19.95	19.51
J163533.8+410649.9	J163533.86+410649.6	V* V851 Her	RR*	ELAISN2_00	27	17.82	2.22	3	19.26	2.11	15.74	15.60	15.60
J163545.4+403016.3	J163545.43+403016.7	QSO B1634+406	QSO	ELAISN2_07	26	19.75	0.77	0	-	-	18.40	18.49	18.31
J163609.3+404749.0	J163609.30+404748.7			ELAISN2_00	29	20.32	0.61	0	-	-	16.43	16.02	15.87
J163618.5+415058.3	J163618.51+415058.9	SDSS J163618.51+415058.9	QSO	ELAISN2_08	20	20.01	0.79	3	21.60	0.79	19.34	19.08	19.06
J163627.1+404848.6	J163627.09+404848.9	[VV96] J163627.2+404847	QSO	ELAISN2_00	26	19.84	0.72	22	20.71	1.03	19.99	19.96	20.06
J163629.6+410222.3	J163629.66+410222.4	CXOEN2 J163629.7+410222	X	ELAISN2_00	26	19.57	1.17	22	19.80	1.75	17.98	17.23	16.87
J163631.3+420242.0	1320-0321675	2MASX J16363129+4202429	Sy1	ELAISN2_08	20	19.31	0.94	3	19.75	0.19	14.43	13.18	13.52
J163702.2+413022.4	J163702.20+413022.2	ELAISC15 J163702+413022	QSO	ELAISN2_00	25	19.71	0.84	12	22.13	0.92	19.70	19.11	19.15
J163737.4+403112.1	J163737.33+403113.1			ELAISN2_00	13	19.93	0.73	0	-	-	17.34	17.03	16.93
J163739.4+414347.9	J163739.43+414348.0	ELAISC15 J163739+414348	QSO	ELAISN2_08	19	19.45	0.84	3	20.39	0.16	19.01	18.94	18.94
J163759.1+420336.5	J163759.16+420336.7	SDSS J163759.16+420336.7	QSO	ELAISN2_08	15	19.83	0.65	3	21.50	0.18	19.51	19.23	19.22
J163802.2+402132.6	J163802.24+402132.3			ELAISN2_04	17	19.90	0.92	1	20.68	-	20.39	20.31	19.95
J163827.2+422144.1	J163827.22+422144.4		PQ	ELAISN2_08	13	19.55	0.65	3	21.05	0.21	19.48	19.23	19.29
J163827.8+411142.0	J163827.82+411142.1	V* V855 Her	V*	ELAISN2_00	25	18.61	1.32	5	21.94	1.88	16.09	15.83	15.74
J163847.0+415245.8	J163847.06+415246.0			ELAISN2_08	16	19.90	0.84	3	21.83	0.49	19.54	19.43	19.55
J163850.7+402409.1	1304-0265981			ELAISN2_04	18	18.42	1.90	0	-	-	14.32	13.37	12.27
J163853.2+413932.7	1316-0284553			ELAISN2_08	29	19.97	1.02	0	-	-	12.33	11.34	10.93
J163908.5+402925.2	J163908.46+402925.1		PQ	ELAISN2_04	17	19.84	0.63	1	20.75	-	19.41	19.50	19.40
J163915.8+412833.4	J163915.80+412833.7	ELAISC15 J163915+412834	QSO	ELAISN2_08	9	18.55	1.49	0	-	-	19.13	19.04	18.90
J163938.1+410646.2	1311-0271661	V* AF Her	RR*	ELAISN2_00	13	15.11	1.88	11	16.52	6.02	13.34	13.07	12.19
J163952.7+420951.6	J163952.76+420951.7			ELAISN2_08	19	18.29	1.75	1	22.35	-	15.88	15.80	15.81
J164009.9+413720.4	J164009.93+413720.4	[CCH92] 1638.5+4143		ELAISN2_03	17	20.20	0.70	1	20.85	-	19.97	19.72	19.72
J164032.8+403705.7	1306-0268136	V* AG Her	RR*	ELAISN2_04	16	14.70	1.90	1	21.73	-	13.27	13.07	12.82
J164106.8+404225.2	1307-0268106	GSC 03074-00114		ELAISN2_04	10	15.70	0.87	1	17.93	-	14.00	14.13	13.88
J164117.7+401921.6	1303-0266136			ELAISN2_04	8	19.99	0.78	0	-	-	12.49	10.92	10.14
J164135.2+413806.9	J164135.27+413807.2	[VV2006c] J164135.2+413807	Sy1	ELAISN2_03	13	20.00	1.00	3	20.42	0.18	19.78	19.57	19.42
J164238.6+395245.5	1298-0277721			ELAISN2_04	3	16.48	1.47	0	-	-	13.19	13.56	12.94
J164337.5+411857.6	1313-0274769			ELAISN2_03	16	18.34	0.86	0	-	-	13.12	12.62	11.35
J164536.6-014631.6	0882-0315863			G11_056023_NGC6218	6	19.68	1.11	0	-	-	16.87	16.44	15.56
J164634.7+350317.8	J164634.71+350317.6	FIRST J164634.6+350317	QSO	DEEPZLE_01	45	20.17	0.62	30	21.59	0.41	19.52	19.43	19.55
J164637.6+345350.2	J164637.50+345348.9	2MASX J16463750+3453488	Gal	DEEPZLE_01	47	18.09	0.64	32	18.25	0.89	19.06	18.84	18.62
J164714.3-020035.7	0879-0410799			G11_056023_NGC6218	7	19.77	1.09	0	-	-	-	15.29	-
J164718.2-015603.4		Cl* NGC 6218 KUST 343		G11_056023_NGC6218	14	17.31	1.16	0	-	-	-	-	-
J164718.8-015221.4	0881-0332822	Cl* NGC 6218 KUST 346		G11_056023_NGC6218	7	19.38	1.03	0	-	-	14.75	14.48	15.19
J164725.0-015505.9	0880-0363588			G11_056023_NGC6218	8	19.02	0.88	0	-	-	12.35	11.90	15.98
J164727.8-020040.7	0879-0411347			G11_056023_NGC6218	11	18.37	2.11	0	-	-	18.80	16.41	-
J164733.2+350542.0	J164733.23+350541.5	SDSS J164733.23+350541.5	QSO	DEEPZLE_01	44	19.97	0.69	31	21.34	1.57	19.89	19.89	20.11
J164737.4+351433.3	J164737.38+351432.9		PQ	DEEPZLE_01	47	19.62	0.64	32	20.30	0.40	20.30	19.59	19.26
J164816.9+343745.2	J164816.98+343745.2	2MASS J16481695+3437453	QSO	DEEPZLE_01	47	19.89	0.82	31	22.03	1.22	19.19	18.84	18.79
J164828.0+344847.8	J164828.07+344847.7			DEEPZLE_01	47	19.38	1.24	8	23.01	1.30	16.68	16.43	16.33
J164858.5+344839.5	1248-0246917			DEEPZLE_01	46	19.80	0.81	15	21.83	2.24	15.25	13.92	13.40
J164921.1+350323.6	J164921.16+350323.6			DEEPZLE_01	42	19.61	0.87	32	20.76	0.46	19.48	19.34	19.40
J164922.3+344431.1	J164922.35+344430.7			DEEPZLE_01	41	20.01	0.86	28	20.67	0.54	20.37	20.44	20.15
J164935.0+351333.1	J164934.98+351333.2			DEEPZLE_01	37	20.37	0.61	25	22.24	0.78	21.18	21.08	20.81
J164939.8+345819.1	J164939.82+345819.0	V* HL Her	RR*	DEEPZLE_01	54	17.31	2.40	12	18.31	4.22	16.11	15.85	15.76
J165153.4-223952.2	0673-0467905			G11_056025_NGC6235	24	18.39	1.91	0	-	-	15.60	14.69	14.29
J165329.3-221055.4	0678-0481542			G11_056025_NGC6235	15	19.58	0.96	0	-	-	15.98	14.85	-
J165336.1-221418.6	0677-0475777			G11_056025_NGC6235	20	20.08	0.74	0	-	-	16.10	14.70	14.38
J165420.0-221637.3	0677-0476678			G11_056025_NGC6235	22	20.28	0.62	0	-	-	15.24	13.82	13.45

Table 2—Continued

GALEX	SDSS or <i>USNO-B1</i>	SIMBAD	Type	Field	N_{det}	NUV_{max}	Δm	N_{det}	FUV_{max}	Δm	g or B	r or R	i or I
J221625.8-182135.6	<i>0716-0887449</i>			CFHTLS4	40	20.22	0.76	34	21.07	1.37	<i>19.90</i>	<i>20.36</i>	-
J221641.6-173252.2	<i>0724-1157703</i>			CFHTLS4	45	19.77	0.77	40	20.08	0.97	-	<i>19.33</i>	<i>18.80</i>
J223518.3+134008.5	J223518.33+134008.2	QSO B2232+1324	QSO	CCS_Q2233	27	20.03	0.76	3	23.33	0.45	19.06	18.83	18.79
J223601.0+134711.5	J223601.09+134711.1			CCS_Q2233	27	19.16	0.91	14	22.03	1.35	15.98	15.90	15.91
J224029.0+120056.3	<i>1020-0738869</i>			CCS_DSF2237	19	17.56	0.85	19	19.69	2.70	<i>15.73</i>	<i>14.59</i>	<i>14.37</i>
J224143.6+115326.2	<i>1018-0688549</i>			CCS_DSF2237	14	17.08	1.27	12	20.03	3.38	<i>14.27</i>	<i>14.18</i>	<i>13.91</i>
J225334.9-394830.4	<i>0501-0831641</i>			EISD1AB	32	20.01	0.92	32	20.76	1.74	<i>20.16</i>	<i>19.55</i>	<i>18.58</i>
J225439.0-395240.8	<i>0501-0831843</i>			EISD1AB	24	19.83	0.67	24	20.83	1.19	<i>20.02</i>	<i>19.87</i>	<i>18.58</i>
J234959.3-434817.8	<i>0461-0761490</i>			QSOHE2347	22	17.09	0.86	10	20.89	0.97	<i>14.21</i>	<i>13.57</i>	<i>12.77</i>
J235249.2-104826.7	J235249.14-104828.4	SDSS J235249.14-104828.4	QSO	UVE_A2670	5	20.15	0.67	0	-	-	19.23	19.08	18.88

Note. — PQ in Column 4 denotes a 'possible quasar' determined from GALEX and SDSS photometry, as described in the text

Table 3. Probable RR
Lyrae and Short Period
Variables

SDSS
J105622.28+570521.9
J105513.80+564747.5
J164939.82+345819.0
J164828.07+344847.7
J100133.25+014328.5
J104844.20+581538.6
J171753.63+594827.0
J223601.09+134711.1
J103759.47+581212.7
J102641.84+572858.4
J103720.93+591653.5
J104803.05+554210.0
J081226.37+033320.1
J104707.59+053349.2
J105130.92+043801.5
J105044.46+045115.7
J171008.92+585113.2
J171250.85+582748.3
J203958.85-010714.5
J204024.29-010950.6
J141949.62+530554.7
J163533.86+410649.6
J163827.82+411142.1
J160857.87+524151.3
J160902.80+524224.3
J161503.00+563006.8
J163017.46+405425.7
J160713.78+555132.5
J161129.86+534345.8
J160324.93+561258.5
J160542.07+564849.3
J163952.76+420951.7
J160759.92+535210.1
J155800.64+535233.6
J120136.95-033328.5
J143823.99+635329.6